ESC European Society of Cardiology

European Heart Journal - Digital Health (2022) **3**, 525–534
https://doi.org/10.1093/ehjdh/ztac058

ORIGINAL ARTICLE

An artificial intelligence-based platform for automatically estimating time-averaged wall shear stress in the ascending aorta

Lei Lv[1,†], Haotian Li[1,†], Zonglv Wu[1,2], Weike Zeng[3], Ping Hua[1,*], and Songran Yang [4,*]

[1]Department of Cardio-Vascular Surgery, Sun Yat-sen Memorial Hospital, Sun Yat-sen University, No. 107 Yan Jiang West Road, 510120 Guangzhou, China; [2]Department of Cardiac Surgery, Guangzhou Women and Children's Medical Center, No. 9 Jinsui Road, 510623 Guangzhou, China; [3]Department of Radiology, Sun Yat-sen Memorial Hospital, Sun Yat-sen University, No. 107 Yanjiang West Road, 510120 Guangzhou, China; and [4]Department of Biobank and Bioinformatics, Sun Yat-sen Memorial Hospital, Sun Yat-sen University, No. 107 Yan Jiang West Road, 510120 Guangzhou, China

Received 6 April 2022; revised 1 September 2022; accepted 6 September 2022; online publish-ahead-of-print 14 October 2022

Aims Aortopathies are a series of disorders requiring multiple indicators to assess risk. Time-averaged wall shear stress (TAWSS) is currently considered as the primary indicator of aortopathies progression, which can only be calculated by Computational Fluid Dynamics (CFD). However, CFD's complexity and high computational cost, greatly limit its application. The study aimed to construct a deep learning platform which could accurately estimate TAWSS in ascending aorta.

Methods and results A total of 154 patients who had thoracic computed tomography angiography were included and randomly divided into two parts: training set (90%, $n = 139$) and testing set (10%, $n = 15$). TAWSS were calculated via CFD. The artificial intelligence (AI)-based model was trained and assessed using the dice coefficient (DC), normalized mean absolute error (NMAE), and root mean square error (RMSE). Our AI platform brought into correspondence with the manual segmentation (DC = 0.86) and the CFD findings (NMAE, 7.8773% ± 4.7144%; RMSE, 0.0098 ± 0.0097), while saving 12000-fold computational cost.

Conclusion The high-efficiency and robust AI platform can automatically estimate value and distribution of TAWSS in ascending aorta, which may be suitable for clinical applications and provide potential ideas for CFD-based problem solving.

* Corresponding author. Tel: +86 13 609716875, Fax: +86 20 81332199, Email: huaping@mail.sysu.edu.cn (P.H.); Tel: +86 13926168990, Fax: +86 20 81332199, Email: yangsr@mail.sysu.edu.cn (S.R.)

†Lv and Li contributed equally to this work.

Graphical Abstract

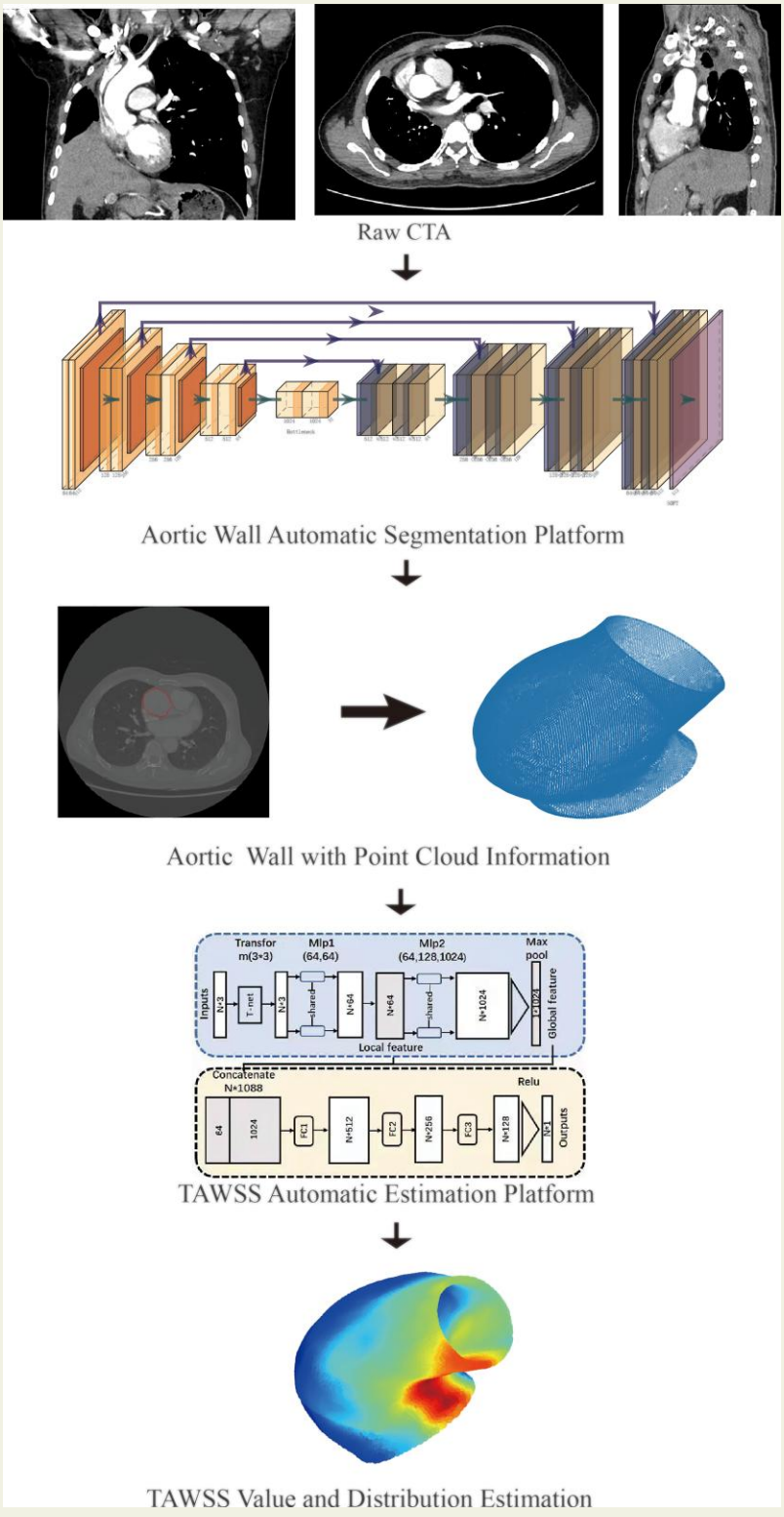

Keywords Aortopathy • Time-averaged wall shear stress • Thoracic computed tomography angiography • Deep learning • Computational fluid dynamics

Introduction

Aortopathies are a group of disorders characterized by aneurysms and dilation of the aorta, which can eventually lead to catastrophic rupture or dissection.[1] Surgical therapy is currently the most common treatment for aortopathies, with the greatest aneurysm diameter serving as an intervention indicator.[2] However, it has been reported that at least half of patients who developed acute aortic syndrome had an aortic size that fell below the threshold for surgical intervention.[3] As a result, researchers are working to develop a variety of evaluation indicators to predict the risk of adverse events in patients with aortopathies.

Haemodynamics indexes, particularly wall shear stress (WSS), defined as the parallel frictional force exerted by blood flow on the endothelial surface of the arterial wall, have been identified as potentially useful metrics to evaluate the risk of aortopathies.[4] Time-averaged wall shear stress (TAWSS), defined as the WSS averaged over the cardiac cycle, is regarded as an important indicator of aneurysm progression. Studies indicated that increased TAWSS of ascending aortic aneurysms was associated with adverse vascular remodelling and mechanotransduction,[5] being correlated with rupture properties in ascending aortic aneurysm.

TAWSS in ascending aorta cannot be measured directly, so it must be combined with computational fluid dynamics (CFD) technology.[6] Some studies have used CFD to obtain aortic geometries[7] from medical imaging data (e.g. MRI, CT, etc.) and estimate haemodynamics parameters that regarded as pathological characteristics of the progression, rupture risk and efficacy evaluation of aortic aneurysm.[8] However, the cost of modelling cardiovascular haemodynamics with available computational resources is prohibitive to incorporating CFD into clinical practice.[9] Obtaining precise haemodynamic parameters, such as TAWSS with low cost is crucial for aortic disease.

The development of artificial intelligence (AI), particularly deep learning (DL), enhances our abilities to address the above challenges.[10] Previous studies have proved that DL can reduce calculation costs in CFD while maintaining accuracy.[11,12] However, many previous studies have used simplified models, constant boundary conditions to reduce computational cost, which resulted in prediction biases.[13,14] Few studies have included automatic segmentation into DL-based CFD analysis, which may increase time costs and contribute to human interference. Therefore, it is necessary to find a new, rapid, and high precision AI-based platform that can automatically identify medical images and predict TAWSS.

In this study, we designed a rapid, end-to-end, and pixel-wise AI-based platform, containing automatic segmentation platform of aortic wall and TAWSS estimation platform, to estimate the distribution of TAWSS in ascending aortas via our own personalized dataset (*Figure 1*). This platform, to the best of our knowledge, was the first to provide a completely end-to-end, efficient, and accurate TAWSS estimation algorithm, which may be more suitable for clinical applications and provide potential ideas for CFD-based problem solving via DL.

Methods

Data

A total of 185 individuals with normal aorta or aortopathies aged 18 years or older were recruited from our centre from 2017 to 2021, with 154 passed quality control (79 normal and 75 aortopathies). Two experienced clinicians investigated and included raw chest and total aortic computed tomography angiographies (CTAs) with the diagnosis of normal ascending aorta (maximum diameter of ascending aorta < 35 mm without abnormal aorta, such as acute aortic syndrome or dissection), dilation (maximum diameter of ascending aorta ≥ 35 mm), and other aortopathies, such as acute aortic syndrome and dissection. Supplementary material online, *Figure S1* depicted the inclusion and exclusion of patients' data.

The experimental scheme and related details of this study were conducted following the Declaration of Helsinki and approved by the Institutional Ethics Committee of Sun Yat-sen Memorial Hospital of Sun Yat-sen University (SYSEC-KY-KS-2021-051). The requirement for informed consent in retrospective cohorts was waived. The Standards for Reporting of Diagnostic Accuracy reporting guideline was used for the reporting of this study.

Computational fluid dynamics analysis of ascending aorta

CFD analysis consists primarily of the following steps: manual aortic segmentation and refining, the discretization technique of finite volume method (FVM), boundary condition setting, transient state CFD calculation and residual monitoring, result acquisition and post-processing.[15–17] We used FVM discretization technique to simulate the ascending aorta from the sinotubular junction (STJ) to the beginning of the brachiocephalic trunk in each case. All cases were treated as transient states with predefined boundary conditions. For residual monitoring, root mean square (RMS) is utilized to ensure that the residual of each time step was smaller than 10^{-6}. *Figure 2* depicts the flow chart of the overall process and detailed information were described in Supplementary material online, *Figure S2*.

Architecture of time-averaged wall shear stress estimation platform

Splitting of data set

For the automatic segmentation platform and the TAWSS automatic estimation platform, the entire dataset from 154 patients was divided into two parts: training set (90%, $n = 139$), and testing set (10%, $n = 15$).

Image pre-processing

To facilitate image segmentation, images were pre-processed by limiting CT intensities, normalizing, resampling and sorting[18] (Supplemental material). All images were sorted along the z-axis and resized to 512512 by the round interpolation.

The pre-processing in point clouds derived from aortic wall segmentation included normalization and down-sampling to 10 000 points per case (Supplemental material), which can make a balance between the calculation cost and accuracy.[19] In addition, we expanded the data by using 10 different initial points in down-sampling, which resulted in a totxal of 1390 point clouds.

Architecture segmentation network development

A U-net-based architecture was adopted for DL-based automatic segmentation (Supplemental material).[20,21] We used the following parameters for U-net model: initialized with random weights, number of epochs = 100, batch size = 16, RMSprop optimizer[22] with learning rate = 0.01, and dice loss as evaluation. The network with the smallest dice loss was chosen and then each case's point clouds were output.

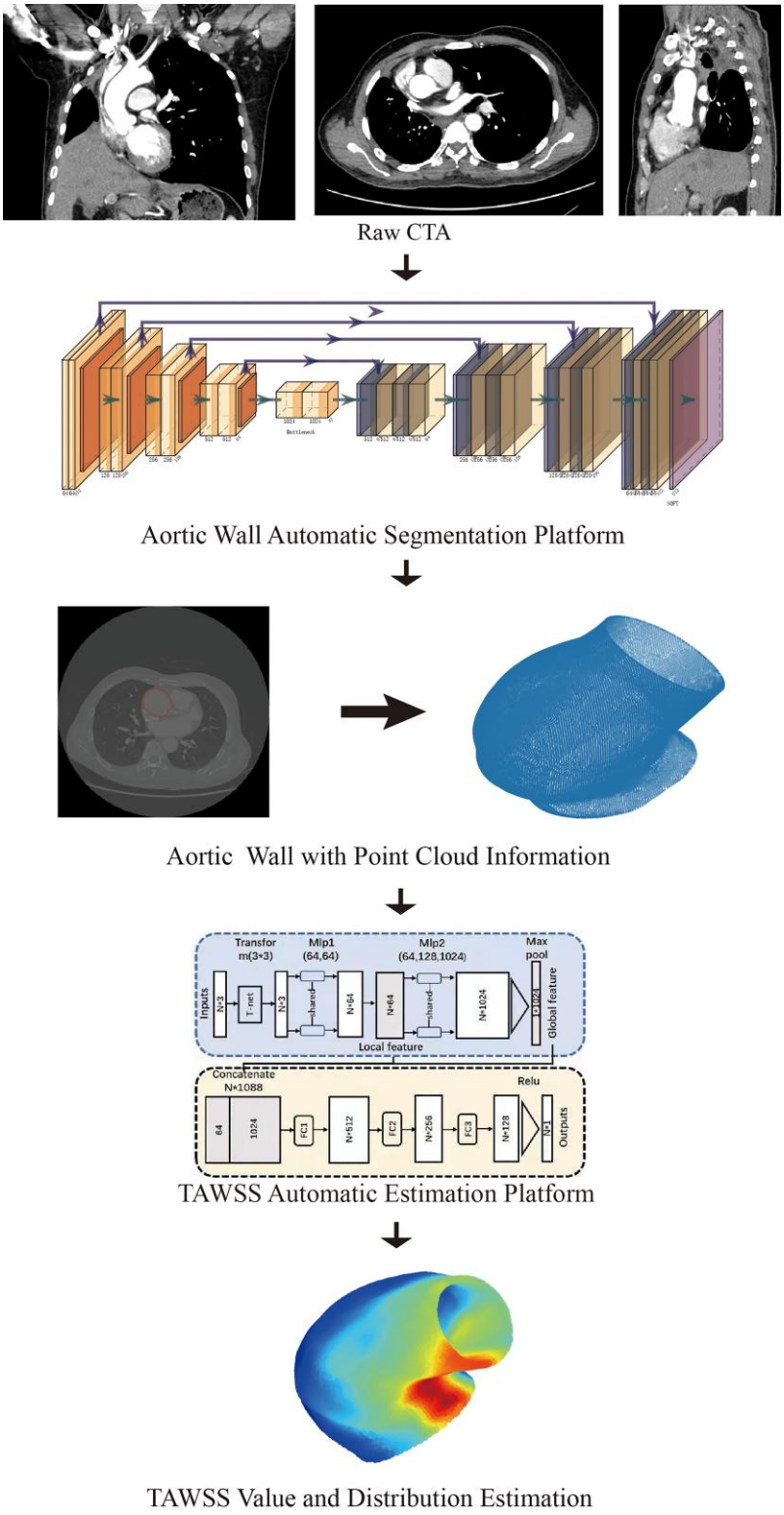

Figure 1 The architecture of the platform. The purpose of this platform is to output the time-averaged wall shear stress values and distribution of the ascending aorta wall in the original computed tomography angiography image. Briefly, the network consists of two parts. The first part is automatic extraction of the aortic wall, and the coordinate information for each point in the point cloud (right) is retrieved from the vessel wall (left). The second is the time-averaged wall shear stress automatic estimation platform. After extracting the coordinate information of ascending aorta wall from the first part, we carried out the time-averaged wall shear stress estimation of each point through the PointNet-based deep learning algorithm, and finally the time-averaged wall shear stress distribution and values of ascending aorta are output. CTAs, computed tomography angiographies; TAWSS, time-averaged wall shear stress.

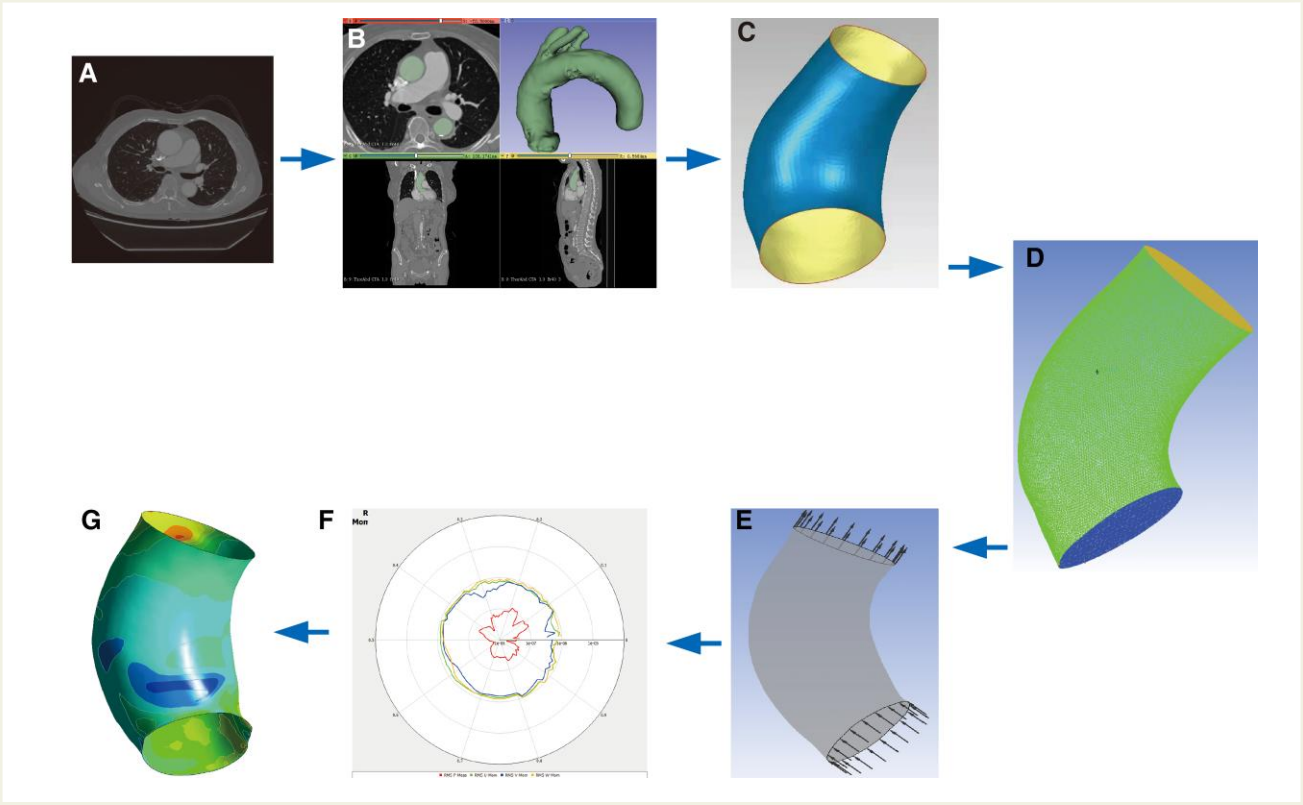

Figure 2 The process of computational fluid dynamics analysis and time-averaged wall shear stress calculation. Shortly, we first labelled the mask of aorta, containing aortic root, aortic sinus, sinotubular junction, ascending aorta, arch, descending aorta and main branches (*B*) from raw computed tomography angiography (*A*). Then ascending aortas were cropped, smoothed and refined (*C*). Tetrahedral meshes and six boundary-fitted prism layers for every case were generated (*D*). And boundary conditions were assigned to each case (*E*). Root mean ssquare was used to monitor the calculation process (*F*). Only when the root mean square value for a timestep was less than 10^{-6} can we carry out the calculation for the next timestep. Lastly, the calculation results, including time-averaged wall shear stress, wall shear stress, and so on, were obtained after post-processing (*G*). CFD, computational fluid dynamics; CTA, computed tomography angiographies; RMS, root mean square; STJ, sinotubular junction; TAWSS, time-averaged wall shear stress; WSS, wall shear stress.

Architecture of time-averaged wall shear stress automatic estimation platform

High-density point clouds {Pi | i = 1, …, N} generated from segmentation were vectors that contained spatial coordinates (x, y, z) as well as hemodynamic indexes such as TAWSS at that position. To analyze these chaotic, sparse, and linked point clouds, we adopted PointNet,[23] a network that can recognize spatial information, detailed architecture of which were shown in Supplemental material.

For training, we utilized a 5-fold cross-validation to ensure that the hyperparameters were adequate. Hyperparameter tweaking and network fitting ability were gauged by comparing their average loss across all five validations (see Supplementary material online, *Figure S6*). We used the following parameters: initialized with random weights, batch size = 16, Adam optimizer with learning rate = 0.01,[24] Cosine annealing decay as attenuation, and mean square error (MSE) as loss function.

Definition of error functions

Dice coefficient (DC) was used to evaluate our performance of segmentation.[25] Then, we chose normalized mean absolute error (NMAE)[26] and root mean square error (RMSE)[27] as our error functions to evaluate the accuracy of the TAWSS estimation platform based on the evaluation criteria in the literature. The error of the DL prediction relative to the ground truth was described using NMAE. See Supplemental material for the calculation formula of the above indicators.

Statistical analysis

Statistical analysis was performed using Python version 3.8. Categorical variables were expressed as counts (percentage), and continuous variable as mean ± SD or median [interquartile range (IQR)]. The Spearman correlation's test between automatic estimation platform prediction and ground truth (CFD result) were similarly evaluated. A *P* value < 0.05 was regarded as significant.

Result

Patients' characteristics and result of computational fluid dynamics-based simulation modelling

A total of 154 patients were eligible for this study (see Supplementary material online, *Table S1*). Compared with group of aortopathies and normal controls, there were no statistically significant differences among genders, ages, or devices. There was no

statistical difference between the training set and the test set either. After calculating, all the cases' RMS of each time step were under 10^{-6} and achieved convergence, which ensured the accuracy of ground truth. The residual monitoring plots and TAWSS distribution at different time points in one cardiac cycle among different diseases were depicted in Supplementary material online, *Figure S3* and *S4*.

Results of automatic segmentation prediction

We examined the best weight on the test set after training the neural network and obtained DC of 0.86. *Figure 3* depicted comparisons of the raw CTAs, manual labels, and automatic segmentations, while Supplementary material online, *Figure S7* presented the voxel level consistency in a Bland-Altman plot between segmentation platform and ground truth.

At this point, we have successfully segmented the anatomy of the ascending aorta, which will replace manual segmentation, and we can convert the segmented images into point cloud.

Results of time-averaged wall shear stress automatic estimation platform

After about 6000 iterations, the loss function fully converged, resulting in a value of 0.003 (see Supplementary material online, *Figure S6*). By comparing the AI-predicted value and distribution of TAWSS in ascending aorta with the ground truth in diverse clinical states including normal (*Figure 4A*), dilation (*Figure 4B*) and patient with significant aortic sinus (56 mm) and aorta (52 mm) dilatation with Marfan syndrome (*Figure 4C*) cases, we found that our platform performed well in predicting the value and distribution of TAWSS in both healthy individuals and aortopathies. See Supplemental material for detailed discussion of flow field characteristic distribution. *Table 1* displayed the NMAE, RMSE and the correlation coefficient between the predicted value and the ground truth among the whole test, normal individuals and aortopathies. Then, by calculating the absolute value of the difference between the predicted value and the ground truth, we discovered that the error was less than 0.2 Pa in most areas, indicating that our model's calculation results were accurate, but the error at the entrance and outlet were relatively large (over 0.5 Pa). In the limitations section below, we provided detailed explanations.

Deep learning improves computing performance

After training, it took 10.84 s/patient (0.09 s/slice) for segmentation and 1.43 s/patient to calculate TAWSS by using a computer with an Intel core i7-10700kf 3.8 Ghz and a NVidia GeForce GTX 3070 GPU, while the whole process manual calculation time for each patient cost about 280 min on the same environment. In comparison to the traditional CFD method, which requires repetitive manual annotation and complex simulated derivation, our platform has a much lower computational cost.

Discussion

In this study, we built a fast, end-to-end, and pixel-wise AI platform that can automatically estimate TAWSS of ascending aorta from CTA. Our platform had two major components: an automatic segmentation platform that could generate 3D coordinate information of the aortic wall via CTA, and a TAWSS estimation platform which took the above-mentioned 3D coordinate and output TAWSS of each node. We demonstrated that the AI platform can properly and quickly estimate complex 3D hemodynamics, providing great application value in scientific research and clinical fields.

TAWSS is an important potential metric for assessing the risk of aortopathies,[8] which currently estimated from medical images due to the lack of direct measurement *in vivo*.[6] Several studies have demonstrated that accurate simulation of hemodynamics can be considered the ground truth.[28] Currently, CT is most frequently chosen as the initial test for the worldwide hospitals of all levels[29] with reliable image quality, fast inspection, and low costs, which is suitable for the hemodynamic index calculation and model reconstruction. To ensure authenticity and reliability of the original data, all images were derived from CTA of in our centre.

Several changes were made during the CFD process in this study to improve computational efficiency based on the relevant parameters reported in previous literature as well as the actual situation. For example, for our research, we segmented ascending aorta from the STJ to the beginning of the brachiocephalic trunk, which is currently used to describe the characteristics of the flow field of the human ascending aorta, analyze how different surgical methods such as the David procedure affect hemodynamics, and predict the outcomes, demontrating that our models were available.[30–32] Blood was a non-Newtonian fluid,[29] but we idealized it as a Newtonian fluid in the ascending aorta [blood is incompressible in the ascending aorta, the aortic wall is non-slip with a large diameter (>30 mm), and the deformation is negligible].[17] The velocity–time curve at inlet and the pressure-time curve at outlet were simplified and re-fitted based on the numerical results reported in the literature[15,17,29] to improve computational efficiency, mimic the hemodynamic characteristics of the aorta as much as possible, and avoid the risk of curve overfitting caused by the limited cases in the references. In our study, we chose transient state and measurable turbulence model, which brought the boundary conditions and prediction closer to the real state *in vivo*.[33,34] When compared to other similar studies that used real medical imaging data and patient-specific boundary conditions, the value and distribution results of TAWSS in ascending aorta and aortopathies obtained by our CFD procedure were generally consistent with those reported in previous literature[5,35] demonstrating the rationality, accuracy, and efficiency of modelling and calculation. Interestingly, some scholars believe that the rationale of integrating assumptions employed with surrogate models for the parameter calibration makes the approach robust, and the consistency of our CFD results with previous studies validated this remark to some extent.[36] Although a high-performance computer was offered, it cost about 280 min to complete each case, which was far from satisfaction. It was necessary for us to find an accurate and fast TAWSS estimation strategy to meet the need of clinic practice.

Some studies tried to solve this kind of problem via DL. Mazian Raissi *et al.*[12] designed Hidden fluid mechanics to solve Navier–Stokes equations and CFD problem, and this landmark work made it possible to address the problem of extracting the velocity and pressure fields directly from the images. In the field of aortic CFD, Liang *et al.*[26] firstly built a DL method to estimate the distribution of

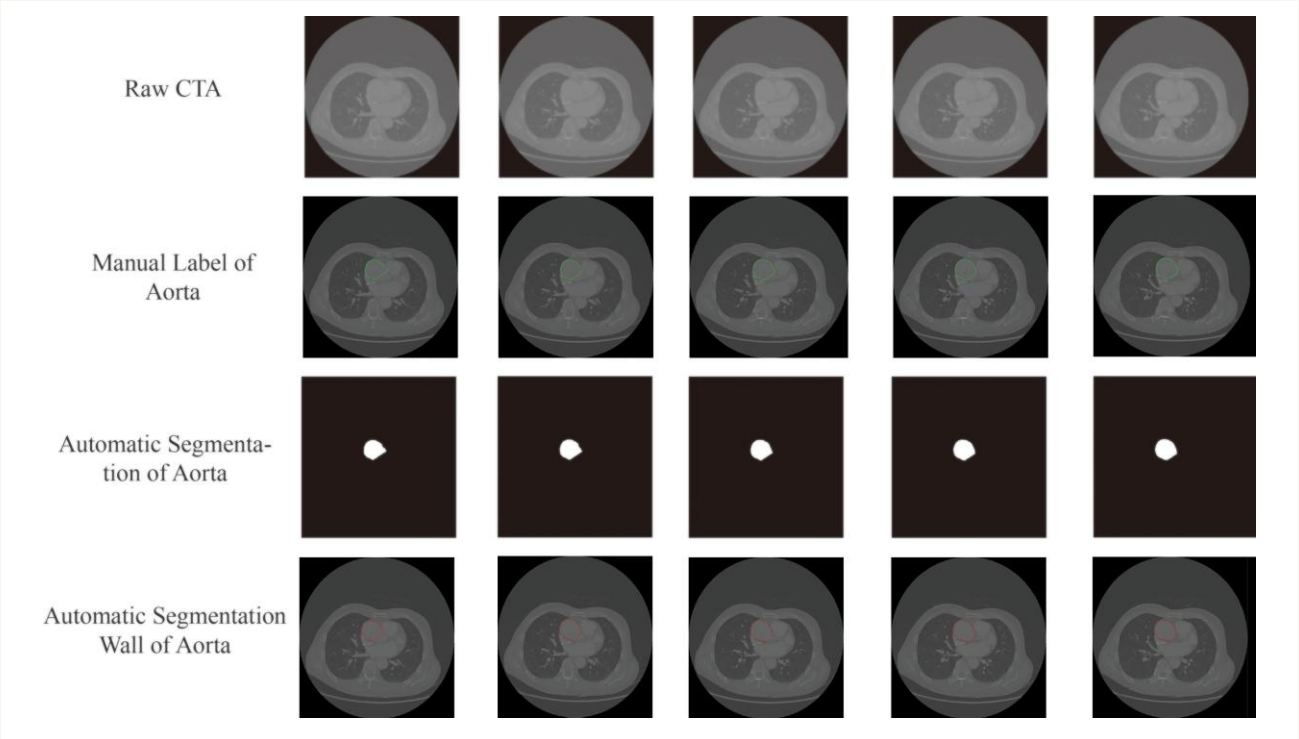

Figure 3 The results of ascending aorta automatic segmentation. The first line shows the raw computed tomography angiography of ascending aorta, and we manually labelled the wall of aorta (the second line). After training, the mask of aorta (the third line) and the aortic wall (the last line) can be extracted automatically. CTAs, computed tomography angiographies.

pressure in aorta, but it was only suitable for ideal aorta, not for the whole complex cardiovascular system, especially for aneurysm. Gaoyang Li *et al.*[11] provided a new idea of point cloud-based DL network. However, the ascending aorta had a high MSE, and the turbulence model did not fit the ascending aorta's haemodynamic properties. To address these flaws, we constructed a DL network based on the framework of PointNet, modified the network by adding a Rectified Linear Unit layer and altered the prediction of probability to the TAWSS. After modification, the platform attained correspondence between the model geometry and its TAWSS distribution, which simplified the entire CFD calculation process a lot while ensured accuracy. Meanwhile, compared with previous studies, our model can accurately estimate TAWSS distribution and values under various disease conditions, such as aneurysm and Marfan syndrome, with strong generalization ability and wide application potential.

In previous DL studies, researchers provided rapid, end-to-end, identification networks for cardiovascular structures from CCTAs or MRI.[21,37] However, there is few articles associated segmentation networks with CFD in the procession of drawing geometric models, and cardiovascular structures are usually identified by semi-automatic methods. These methods are time-consuming and dependent on the clinical experience of the operator, which meant the results varies between senior clinicians and junior clinicians. To solve these problems, we constructed a U-net-based automated segmentation network for wall of ascending aorta, which can meet the needs for subsequent network, such as fast, accurate, and low cost. In our study, aortic segmentation performed consistently well in comparison to similar studies in most regions.[38] The prediction results at the inlet and outlet, on the other hand, are relatively poor, owing to the considerable variance of the above regions and cardiac motion. Poor performance due to motion and artery ostium variation is a common issue in the field of cardiovascular deep learning, and it is inevitable in the absence of ECG-gated imaging data.[39,40]

As far as we know, our platform was the first-reported end-to-end, pixel-wise platform combining ascending aorta segmentation with TAWSS estimation and can be widely used in clinical practice for high accuracy, convenient, and rapidity.

Study limitations

First is the lack of personalized or dynamic boundary conditions. Because of the lack of specific and individual patient flow data in our centre, exact values of the boundary conditions were derived from the published literatures.[16,17] This would result in simulation results that do not perfectly reflect the dynamic changes in haemodynamics. In our platform, we found some error predictions in the inlet and outlet, which may result from the re-fitted velocity–time curve and the haemodynamic characteristics at this location did not match the geometric characteristics completely. Moreover, the image data were from thoracic CTA in the absence of ECG-gated and prone to artefacts caused by heart motion, which led to bias. This bias implied that there were differences in the data distribution

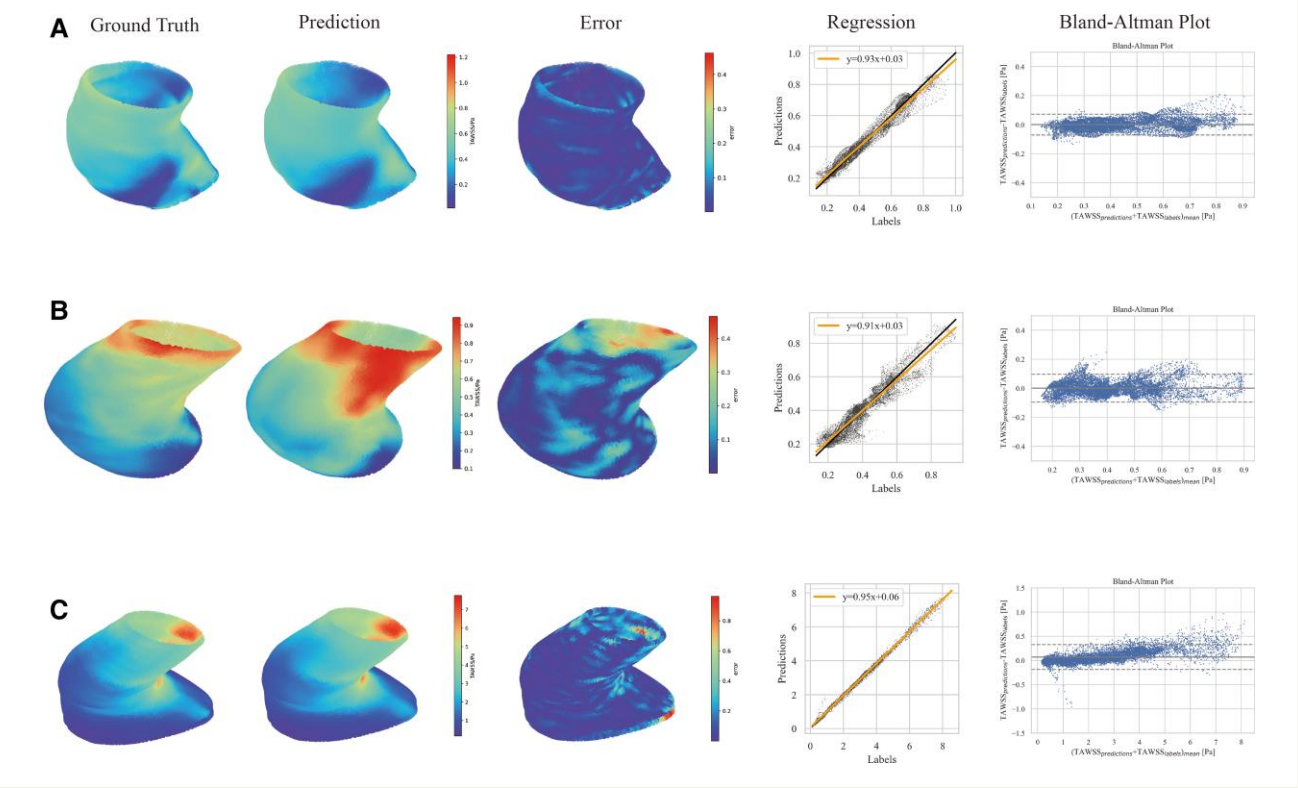

Figure 4 The results of time-averaged wall shear stress estimation platform. The figure shows the estimated results of patients with three different states. (*A*) A healthy volunteer (diameter of aorta = 32 mm). (*B*) An aneurysm patient (diameter = 47 mm), and (*C*) a patient with significant aortic sinus (56 mm) and aorta (52 mm) dilatation with Marfan syndrome. The first column was the ground truth calculated from computational fluid dynamics. The second column was the results of this platform, both distribution and values of which had a good consistency with the ground truth. The third column was the error of each estimation. The final column had the Bland–Altman plots, reflecting the WSS derived using both CFD and deep learning techniques. This model had a high accuracy in time-averaged wall shear stress estimation along with various aortic diseases. CFD, computational fluid dynamics; TAWSS, time-averaged wall shear stress.

Table 1 Accuracy of test data in time-averaged wall shear stress estimation platform

	NMAE[a]	RMSE[b]	*r*[c]	*P*
Total	7.8773%±4.7144%	0.0098 ± 0.0097	0.8124 ± 0.1639	< 0.001
Normal	8.6412%±4.7289%	0.0063 ± 0.0049	0.7777 ± 0.1702	< 0.001
Aortopathies	7.2087%±4.5987%	0.0128 ± 0.0117	0.8428 ± 0.1516	< 0.001

[a]NMAE, normalized mean absolute error.
[b]RMSE, root mean square error.
[c]*r*, the correlation coefficient between predicted value and ground truth.

for the neural network and required a higher data size for fitting the CFD results. Besides, the image quality in the ascending aortic plane was better than the STJ, caused the higher error of TAWSS estimation in the STJ. In fact, poor performance due to motion and artery ostium variation is a common issue in the field of cardiovascular deep learning, and further exploration of practical solutions is still needed.[39,40]

Second, the present study retrospectively collected CTA data from a single centre before rupture event, and the number of enrolled patients was relatively small. However, based on deep learning, these platforms were greedy for data which meant our results must be verified in a larger cohort including the cost-effectiveness of the current approach.[41]

Conclusions

In this research, we built a fast, end-to-end, and pixel-wise AI platform, containing automatic segmentation platform of aortic wall and TAWSS estimation, which can automatically estimate values and distribution of TAWSS in ascending aorta with various disease

type from CTA. The high-efficiency and robust platform may be suitable for clinical applications and provide potential ideas for CFD-based problem solving via deep learning.

Supplementary material

Supplementary materials are available at European *Heart Journal – Digital Health* online.

Author contributions

P.H. and S.Y. designed research; L.L., H.L., Z.W., and S.Y. performed research; L.L., H.L., Z.W., P.H., and S.Y. analyzed data; and L.L., H.L., P.H., and S.Y. wrote the paper.

Funding

This work was supported by the National Natural Science Foundation of China (NSFC No. 81771165), the Natural Science Foundation Project in Guangdong province, China (Grant Nos. 2020A1515010233; 2018A030313172), and Guangzhou Science and Technology project of Major Special Research Topics on International Collaborative Innovation (Grant Nos. 201704030032; 201807010010).

Conflict of interest: None declared.

Data availability

The data that support the findings of this study are available on request from the corresponding author upon approval of data sharing committees of the respective institutions.

References

1. Ramanath VS, Oh JK, Sundt TM III, Eagle KA. Acute aortic syndromes and thoracic aortic aneurysm. *Mayo Clin Proc* 2009;**84**:465–481.
2. Erbel R, Aboyans V, Boileau C, Bossone E, Bartolomeo RD, Eggebrecht H, *et al.* 2014 ESC guidelines on the diagnosis and treatment of aortic diseases: document covering acute and chronic aortic diseases of the thoracic and abdominal aorta of the adult. The task force for the diagnosis and treatment of aortic diseases of the European society of cardiology (ESC). *Eur Heart J* 2014;**35**:2873–2926.
3. Svensson LG, Kim KH, Lytle BW, Cosgrove DM. Relationship of aortic cross-sectional area to height ratio and the risk of aortic dissection in patients with bicuspid aortic valves. *J Thorac Cardiov Sur* 2003;**126**:892–893.
4. Youssefi P, Gomez A, Arthurs C, Sharma R, Jahangiri M, Alberto Figueroa C. Impact of patient-specific inflow velocity profile on hemodynamics of the thoracic aorta. *J Biomech Eng* 2018;**140**:0110021–0110214.
5. Pasta S, Agnese V, Gallo A, Cosentino F, Di Giuseppe M, Gentile G, *et al.* Shear stress and aortic strain associations with biomarkers of ascending thoracic aortic aneurysm. *Ann Thorac Surg* 2020;**110**:1595–1604.
6. Batchelor GK. *An Introduction to fluid dynamics*. Cambridge: Cambridge University Press; 2000.
7. Tang CX, Liu CY, Lu MJ, Schoepf UJ, Tesche C, Bayer RRII, *et al.* CT FFR for ischemia-specific CAD with a new computational fluid dynamics algorithm: a Chinese multicenter study. *JACC Cardiovasc Imaging* 2020;**13**:980–990.
8. Hoi Y, Meng H, Woodward SH, Bendok BR, Hanel RA, Guterman LR, *et al.* Effects of arterial geometry on aneurysm growth: three-dimensional computational fluid dynamics study. *J Neurol Neurosurg* 2004;**101**:676–681.
9. Taylor CA, Fonte TA, Min JK. Computational fluid dynamics applied to cardiac computed tomography for noninvasive quantification of fractional flow reserve: scientific basis. *J Am Coll Cardiol* 2013;**61**:2233–2241.
10. He J, Baxter SL, Xu J, Xu J, Zhou X, Zhang K. The practical implementation of artificial intelligence technologies in medicine. *Nat Med* 2019;**25**:30–36.
11. Li G, Wang H, Zhang M, Tupin S, Qiao A, Liu Y, *et al.* Prediction of 3D cardiovascular hemodynamics before and after coronary artery bypass surgery via deep learning. *Commun Biol* 2021;**4**:1–12.
12. Raissi M, Yazdani A, Karniadakis GE. Hidden fluid mechanics: learning velocity and pressure fields from flow visualizations. *Sci* 2020;**367**:1026–1030.
13. Ferez XM, Mill J, Juhl KA, Acebes C, Iriart X, Legghe B, *et al.* Deep learning framework for real-time estimation of in-silico thrombotic risk indices in the left atrial appendage. *Front Physiol* 2021;**12**:6–19.
14. Li G, Song X, Wang H, Liu S, Ji J, Guo Y, *et al.* Prediction of cerebral aneurysm hemodynamics with porous-Medium models of flow-diverting stents via deep learning. *Front Physiol* 2021;**12**:733444(1–13).
15. Febina J, Sikkandar MY, Sudharsan NM. Wall shear stress estimation of thoracic aortic aneurysm using computational fluid dynamics. *Comput Math Methods Med* 2018;**2018**:71263532(1–12).
16. Kalykakis GE, Antonopoulos AS, Pitsargiotis T, Siogkas P, Exarchos T, Kafouris P, *et al.* Relationship of endothelial shear stress with plaque features with coronary CT angiography and vasodilating capability with PET. *Radiology* 2021;**300**:549–556.
17. Midulla M, Moreno R, Baali A, Chau M, Negre-Salvayre A, Nicoud F, *et al.* Haemodynamic imaging of thoracic stent-grafts by computational fluid dynamics (CFD): presentation of a patient-specific method combining magnetic resonance imaging and numerical simulations. *Eur Radiol* 2012;**22**:2094–2102.
18. Moenning C, Dodgson NA, Dodgson N. Number 562 Fast Marching farthest point sampling Fast Marching farthest point sampling. 2003. http://www.cl.cam.ac.uk/http://www.cl.cam.ac.uk/TechReports/ (accessed 20 Oct 2021).
19. Isensee F, Jaeger PF, Kohl SAA, Petersen J, Maier-Hein KH. nnU-Net: a self-configuring method for deep learning-based biomedical image segmentation. *Nat Med* 2021;**18**:203–211.
20. Ma X, Hadjiiski LM, Wei J, Chan HP, Cha KH, Cohan RH, *et al.* U-Net based deep learning bladder segmentation in CT urography. *Med Phys* 2019;**46**:1752–1765.
21. Baskaran L, Maliakal G, Al'Aref SJ, Singh G, Xu Z, Michalak K, *et al.* Identification and quantification of cardiovascular structures from CCTA: an end-to-end, rapid, pixel-wise, deep-learning method. *JACC Cardiovasc Imaging* 2020;**13**:1163–1171.
22. Tieleman T, Hinton G. Lecture 6.5-rmsprop: divide the gradient by a running average of its recent magnitude. *COURSERA: Neural Networks for Machine Learning* 2012;**4**:26–30.
23. Qi CR, Su H, Mo K, Guibas LJ. Pointnet: deep learning on point sets for 3D classification and segmentation (ed.), *Proceedings—30th IEEE conference on computer vision and pattern recognition, CVPR 2017*. Honolulu: Institute of Electrical and Electronics Engineers Inc; 2017. p77–85.
24. Kingma DP, Ba J. Adam: A Method for Stochastic Optimization. 3rd International Conference on Learning Representations, ICLR 2015—Conference Track Proceedings 2014. https://arxiv.org/abs/1412.6980v9 (accessed 20 Oct2021).
25. Sudre CH, Li W, Vercauteren T, Ourselin S, Jorge Cardoso M. Generalised dice overlap as a deep learning loss function for highly unbalanced segmentations. In: *Deep Learn Med Image Anal Multimodal Learn Clin Decis Support* 2017:240–248.
26. Liang L, Liu M, Martin C, Sun W. A deep learning approach to estimate stress distribution: a fast and accurate surrogate of finite-element analysis. *J R Soc Interface* 2018;**15**:20170844(1–10).
27. Chai T, Draxler RR. Root mean square error (RMSE) or mean absolute error (MAE)?—arguments against avoiding RMSE in the literature. *Geosci Model Dev* 2014;**7**:1247–1250.
28. Arzani A, Suh GY, Dalman RL, Shadden SC. A longitudinal comparison of hemodynamics and intraluminal thrombus deposition in abdominal aortic aneurysms. *AM J Physiol-Heart C* 2014;**307**:H1786–H1795.
29. Cong M, Zhao H, Dai S, Chen C, Xu X, Qiu J, *et al.* Transient numerical simulation of the right coronary artery originating from the left sinus and the effect of its acute take-off angle on hemodynamics. Quant. *Imaging* 2021;**11**:2062–2075.
30. Leuprecht A, Perktold K, Kozerke S, Boesiger P. Combined CFD and MRI study of blood flow in a human ascending aorta model. *Biorheology* 2002;**39**:425–429.
31. Berdajs D, Mosbahi S, Forro Z, Burki M, von Segesser LK. Aortic root haemodynamics following david procedure: numerical analysis of 3-dimensional haemodynamics. *Eur J Cardiothorac Surg* 2016;**49**:1588–1598.
32. Dowling C, Gooley R, Mccormick L, Firoozi S, Brecker SJ. Patient-specific computer simulation to predict long-term outcomes after transcatheter aortic valve replacement. *J Cardiovasc Comput Tomogr* 2022;**16**:254–261.
33. De Wilde D, Trachet B, De Meyer G, Segers P. The influence of anesthesia and fluid-structure interaction on simulated shear stress patterns in the carotid bifurcation of mice. *J Biomech* 2016;**49**:2741–2747.
34. Stein PD, Sabbah HN. Turbulent blood flow in the ascending aorta of humans with Normal and diseased aortic valves. *Circ Res* 1976;**39**:58–65.
35. Camarda JA, Dholakia RJ, Wang H, Samyn MM, Cava JR, LaDisa JF Jr. A pilot study characterizing flow patterns in the thoracic aorta of patients with connective tissue

disease: comparison to age- and gender-matched controls via fluid structure interaction. *Front Pediatr* 2022;**10**:772142.
36. Xu H, Piccinelli M, Leshnower BG, Lefieux A, Taylor WR, Veneziani A. Coupled morphological-hemodynamic computational analysis of type B aortic dissection: a longitudinal study. *Ann Biomed Eng* 2018;**46**:927–939.
37. Masutani EM, Bahrami N, Hsiao A. Deep learning single-frame and multiframe super-resolution for cardiac MRI. *Radiology* 2020;**295**: 552–561.
38. Sieren MM, Widmann C, Weiss N, Moltz JH, Link F, Wegner F, Stahlberg E, Horn M, Oecherting TH, Goltz JP, Barkhausen J, Frydrychowicz A. Automated segmentation and quantification of the healthy and diseased aorta in CT angiographies using a dedicated deep learning approach. *Eur Radiol* 2022;**32**:690–701.
39. You S, Masutani EM, Alley MT, Vasanawala SS, Taub PR, Liau J, *et al.* Deep learning automated background phase error correction for abdominopelvic 4D flow MRI. *Radiology* 2022;**302**:584–592.
40. Shin CI, Park SJ, Kim JH, Yoon YE, Park EA, Koo BK, *et al.* Coronary artery lumen segmentation using location-adaptive threshold in coronary computed tomographic angiography: a proof-of-concept. *Korean J Radiol* 2021;**22**:688–696.
41. Cho J, Lee K, Shin E, Choy G, Do S. How much data is needed to train a medical image deep learning system to achieve necessary high accuracy. *ArXiv* 2015;1–10.